CANCER

ITGA5 inhibition in pancreatic stellate cells attenuates desmoplasia and potentiates efficacy of chemotherapy in pancreatic cancer

Praneeth R. Kuninty[1], Ruchi Bansal[1]*, Susanna W. L. De Geus[2]*, Deby F. Mardhian[1], Jonas Schnittert[1], Joop van Baarlen[3], Gert Storm[1,4], Maarten F. Bijlsma[5], Hanneke W. van Laarhoven[5], Josbert M. Metselaar[6,7], Peter J. K. Kuppen[2], Alexander L. Vahrmeijer[2], Arne Östman[8], Cornelis F. M. Sier[2], Jai Prakash[1,6,8†]

Abundant desmoplastic stroma is the hallmark for pancreatic ductal adenocarcinoma (PDAC), which not only aggravates the tumor growth but also prevents tumor penetration of chemotherapy, leading to treatment failure. There is an unmet clinical need to develop therapeutic solutions to the tumor penetration problem. In this study, we investigated the therapeutic potential of integrin α5 (ITGA5) receptor in the PDAC stroma. ITGA5 was overexpressed in the tumor stroma from PDAC patient samples, and overexpression was inversely correlated with overall survival. In vitro, knockdown of ITGA5 inhibited differentiation of human pancreatic stellate cells (hPSCs) and reduced desmoplasia in vivo. Our novel peptidomimetic AV3 against ITGA5 inhibited hPSC activation and enhanced the antitumor effect of gemcitabine in a 3D heterospheroid model. In vivo, AV3 showed a strong reduction of desmoplasia, leading to decompression of blood vasculature, enhanced tumor perfusion, and thereby the efficacy of gemcitabine in co-injection and patient-derived xenograft tumor models.

INTRODUCTION

Pancreatic ductal adenocarcinoma (PDAC) is one of the most devastating cancers, with a 5-year survival rate of less than 8% (*1*). Currently, available therapies are insufficient to substantially halt the growth of PDAC, indicating an unmet clinical need to develop novel therapeutics. PDAC is characterized by abundant tumor stroma (up to 90% of the total tumor mass), which has been shown to promote tumor growth and metastasis, and confer resistance to chemotherapy, as well as act as a physical barrier by preventing tumor delivery of therapeutics (*2*, *3*). Pancreatic tumor stroma is composed of nonmalignant cells such as cancer-associated fibroblasts (CAFs), immune cells, vasculature, and a network of extracellular matrix (ECM), which interact with tumor cells in a bidirectional manner (*2*, *4*). CAFs are key effector cells in the stroma, which produce ECM molecules such as collagen, fibronectin (FN), and laminin and secrete various cytokines and growth factors, which altogether stimulate tumor growth, angiogenesis, invasion, and metastases (*5*). CAFs mainly originate from pancreatic stellate cells (PSCs), the resident mesenchymal cells in the pancreas (*6*, *7*). PSCs are normally present in low numbers in a quiescent form storing vitamin A droplets. However, during malignant transformation, PSCs get activated and transform into myofibroblasts identified by α-smooth muscle actin (α-SMA) expression (*8*). Furthermore, PSCs have been shown to secrete growth factors that induce tumor cell growth, survival, and migration (*9*). In an earlier study, we found an overexpression of miR-199a and miR-214 in PDAC stroma and demonstrated that their inhibition using antagomirs resulted in inhibition of PSC activation, which resulted in reduced protumorigenic response in vitro (*10*). More recently, we have demonstrated that inhibition of PSC activation using natural molecules such as lipoxin A4 or relaxin hormone resulted in inhibition of PSC-induced desmoplasia and tumor growth in vivo in co-injection tumor models (*11*, *12*). Although some reported studies have shown the contrasting effects of stroma on tumor growth (*13*) (*14*), there is a continuously growing literature showing the tumor-promoting role of PSCs and PDAC tumor stroma (*7*). There is a high need to find novel targets in PSCs that can be used to develop novel therapeutics to diminish the tumor-promoting role of tumor stroma in PDAC.

Integrins are heterodimeric transmembrane receptors consisting of α and β subunits, which form a large family of about 24 α and β integrins (*15*, *16*). As cell adhesion receptors, integrins mediate cell-to-cell and cell-to-ECM interactions, but they also play an active role in signal transduction by regulating cytoskeletal organization, cell migration, proliferation, and survival (*15*, *16*). Several integrins, αvβ3, αvβ5, αvβ6, α6β4, α4β1, α11β1, and α5β1, are reported to be overexpressed in various cancer types, being involved in tumor progression through tumor cell invasion and metastases (*16*). Recently, we have also shown the role of integrin α11, a collagen receptor, in activation of PSCs and PSC-induced migration of tumor cells (*17*).

In the present study, we investigated the prognostic and therapeutic role of integrin α5 subunit (ITGA5) in the stroma of pancreatic tumors. ITGA5, together with β1, forms a receptor for FN, which have mainly been explored for their role in malignant tumor cells and tumor vasculature (*15*, *18*, *19*). Here, we showed the overexpression of ITGA5 in the tumor stroma of PDAC patients and correlated it with the overall survival (OS) rate. Then, we examined the role of ITGA5 in human PSCs (hPSCs) in vitro by knocking down

[1]Department of Biomaterials, Science and Technology, Section: Targeted Therapeutics, Faculty of Science and Technology, University of Twente, Enschede, Netherlands. [2]Department of Surgery, Leiden University Medical Center, Leiden, Netherlands. [3]Laboratory Pathology Oost Netherlands (LabPON), Hengelo, Netherlands. [4]Department of Pharmaceutics, Utrecht University, Utrecht, Netherlands. [5]Amsterdam University Medical Centre, University of Amsterdam, Amsterdam, Netherlands. [6]ScarTec Therapeutics BV, Enschede, Netherlands. [7]Department of Nanomedicine and Theranostics, Institute for Experimental Molecular Imaging, RWTH University Clinic, Forckenbeckstrasse 55, 52074 Aachen, Germany. [8]Department of Oncology-Pathology, Cancer Center Karolinska, Karolinska Institutet, Stockholm, Sweden.
*These authors contributed equally to this work.
†Corresponding author. Email: j.prakash@utwente.nl

its expression using short hairpin RNA (shRNA). Next, we investigated the effect of sh-ITGA5 PSCs on tumor growth and desmoplasia in a co-injection (PANC-1 + hPSCs) tumor mouse xenograft model in vivo. Then, we designed a novel short peptidomimetic (AV3) against ITGA5 and examined its therapeutic efficacy in vitro and in vivo in co-injection (PANC-1 + hPSCs and MIA PaCa-2 + hPSCs) and patient-derived xenograft (PDX) models.

RESULTS

Induced expression of ITGA5 in clinical PDAC samples and PSCs

The immunohistochemical analyses for ITGA5 expression showed a strong expression in human PDAC samples, while there was no expression in normal pancreatic tissues (Fig. 1A). Within the tumor region, ITGA5 was largely and differentially expressed in the tumor stroma compared with tumor epithelial cells in which only weak to negligible expression levels were observed (Fig. 1A). In the total sample cohort, the tumor/stroma ratio was found in 89% of the patients. ITGA5 was expressed in 66% of the patients with PDAC, whereas α-SMA was expressed in 85% (table S1). Using double immunofluorescence for ITGA5 (red) and α-SMA (green) immunostainings, we found that about 72% of α-SMA$^+$ cells were positive for ITGA5, while 28% did not express ITGA5 (Fig. 1B). Besides that, there were also some cells only positive for ITGA5 but not for α-SMA (Fig. 1B). In univariate analyses, age and sex did not demonstrate predictive values for OS. However, primary tumor stage, lymph node metastasis stage, margin status, and ITGA5 expression in stromal cells were significantly predictive for OS (table S2). In multivariate analysis, only ITGA5 expression in stromal cells was a significant prognostic factor for OS in pancreatic cancer (table S2). Survival analysis reveals that the overexpression of both α-SMA and ITGA5 (log-rank $P = 0.022$ and 0.008, respectively) was linked to significantly decreased OS (Fig. 1C). In addition, we examined the ITGA5 mRNA expression from the publicly available dataset and found that ITGA5 expression in the tumor was significantly higher than adjacent non-tumor tissue (Fig. 1D). PSCs are considered as the main source for CAFs in pancreatic tumor stroma (*4*, *7*). Upon activation with transforming growth factor–β (TGF-β), PSCs differentiate into α-SMA–expressing myofibroblast-like CAFs and produce abundant ECM (*20*). In this study, we show that quiescent hPSCs upon activation with human recombinant TGF-β developed high expression levels of α-SMA, as shown by immunofluorescence staining (Fig. 1E). These data were also confirmed at protein and mRNA levels using Western blot and quantitative polymerase chain reaction (qPCR) analyses, respectively (Fig. 1, F and G). Furthermore, we found that, in contrast to α-SMA, ITGA5 was also expressed by quiescent hPSCs, but upon activation with TGF-β, the expression levels of ITGA5 were further induced, as shown by immunofluorescence staining, Western blot, and qPCR analyses (Fig. 1, E to G).

ITGA5 knockdown attenuates TGF-β–induced PSC activation

To study the effect of ITGA5 on the activation of hPSCs, we knocked down ITGA5 expression using puromycin-resistant lentiviral shRNA plasmid. The stably shRNA-mediated ITGA5 knockdown (sh-ITGA5) hPSCs showed reduced ITGA5 (Fig. 2A) and α-SMA (Fig. 2B) expression levels compared to the negative control (NC) shRNA (sh-NC). Additional shRNA hairpin was used to show the specificity (fig. S1A). As shown in Fig. 2A (zoomed images), the overexpression of ITGA5 along the actin filaments in the TGF-β–activated hPSCs was lost in sh-ITGA5 hPSCs. The inhibitory effect of ITGA5 knockdown on TGF-β–induced expression levels of ITGA5, α-SMA, and collagen I in hPSCs was confirmed at the protein level using Western blot analysis (fig. S1B). ITGA5-mediated control of α-SMA is in line with the previous study (*21*). Because the activated hPSCs produce abundant ECM during tumorigenesis and attach via adhesion proteins, we investigated the impact of ITGA5 knockdown on ECM and adhesion proteins using a human profiler gene array composed of 84 genes. As shown in Fig. 2C, the expression levels of several genes related to ECM and adhesion molecules were significantly down-regulated (<0.5-fold) in sh-ITGA5 compared to sh-NC hPSCs. Activation of sh-NC hPSCs with TGF-β led to the up-regulation (>2.0-fold) of about 42 genes. Activation of sh-ITGA5 hPSCs with TGF-β did not up-regulate the down-regulated genes (Fig. 2C and data file S1). Furthermore, sh-ITGA5 hPSCs had a significantly reduced mRNA expression of key activation markers such as ACTA2 (α-SMA), Fibronectin1 (FN1), platelet-derived growth factor β receptor (PDGFβR), and other key TGF-β activation markers and signaling molecules, including TGF-β, POSTN, YAP, and CXC12 (fig. S1C). These data indicate that the down-regulation of ITGA5 expression level leads to inhibition of TGF-β–mediated differentiation of hPSC into myofibroblast-like CAFs and thereby inhibits ECM production.

ITGA5 knockdown abrogates hPSC's function via the TGF-β/Smad2/FAK pathway

Integrins are known to control various cellular processes such as migration, cell adhesion, contraction, and proliferation (*16*). We, therefore, investigated whether ITGA5 plays a role in controlling the PSC phenotype. We examined cell-to-ECM and cell-to-cell adhesion using a plate cell adhesion assay and a spheroid assay, respectively. Because ITGA5 is a receptor for FN, we examined the attachment of cells on FN-coated plates. Compared with sh-NC hPSCs, sh-ITGA5 hPSCs attached significantly lesser to FN (Fig. 2D) and also formed significantly lesser compact spheroids after 6 days of culturing (Fig. 2E). Furthermore, ITGA5 knockdown significantly inhibited hPSC proliferation, as shown by 5-bromo-2′-deoxyuridine (BrdU) assay (Fig. 2F), migration (scratch assay, Fig. 2G), and TGF-β–induced contractility in a three-dimensional (3D) collagen gel contraction assay (Fig. 2H). The reduction in migration was not related to the effect on proliferation, as this assay was performed within 15 hours while there was no change in proliferation up to 24 hours (Fig. 2F). These data suggest that ITGA5 plays a crucial role in the regulation of cell adhesion, migration, proliferation, and TGF-β–induced contractility of hPSCs. Having established that ITGA5 knockdown attenuates TGF-β–induced differentiation and phenotypic changes in hPSCs, we examined the potential pathways responsible for these activities. We investigated the effect on the TGF-β signaling pathway, i.e., pSmad2. In addition, ITGA5 is known to act via focal adhesion kinase (FAK) as a canonical pathway, and its cross-talk with TGF-β has also been proposed in the literature (*22*, *23*). We therefore also investigated the effect of ITGA5 knockdown on the FAK pathway. We performed Western blots at early (30 min) and late (48 hours) time points after TGF-β activation. We found that pSmad2 expression was induced at 30 min after TGF-β activation (Fig. 2I). ITGA5 knockdown reduced not only the phosphorylation of Smad2 but also FAK pathways in both non-activated and TGF-β–activated hPSCs (Fig. 2I). In addition, we examined the effect of ITGA5 knockdown on ITGA5-induced direct signaling molecules, i.e., FHL3 (four and

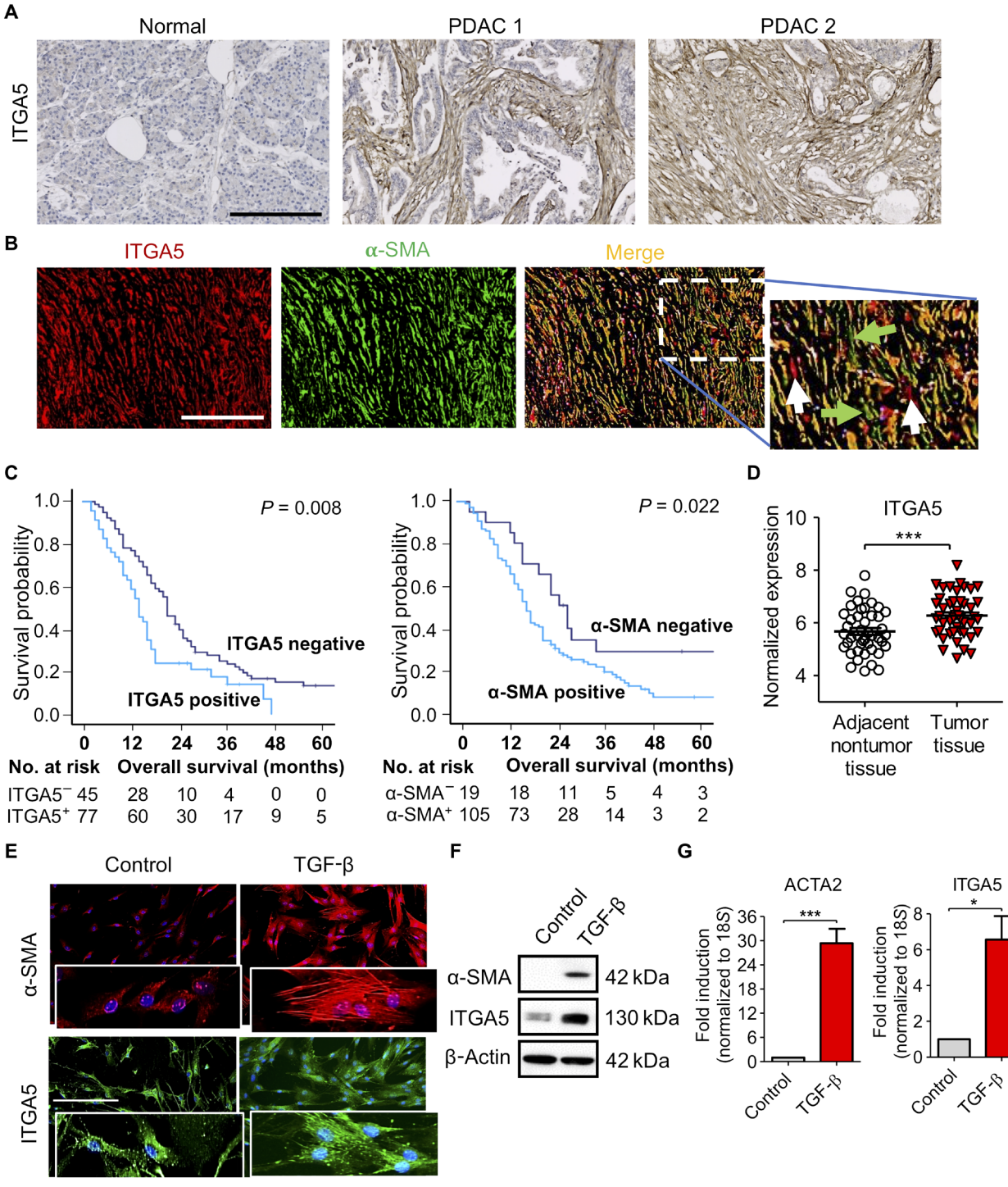

Fig. 1. ITGA5 expression and prognostic value in PDAC and PSCs. (**A**) Immunohistochemical staining for ITGA5 performed on pancreatic tumor and normal pancreas on tissue microarrays (TMAs). Scale bar, 100 μm. (**B**) Double immunofluorescence staining shows ITGA5 (red) and α-SMA (green) with DAPI (4′,6-diamidino-2-phenylindole; blue nuclei) in the PDAC tissue. Scale bar, 100 μm. (**C**) Kaplan-Meier overall survival curves for the stromal expression of ITGA5 and α-SMA in patients with PDAC. Log-rank test was performed to calculate significant differences. Survival analyses were performed using the Kaplan-Meier method. (**D**) Transcriptomic analysis of ITGA5 in publicly available microarray dataset (GSE28735). (**E**) Immunofluorescence staining showing α-SMA and ITGA5 expression levels in hPSCs with or without TGF-β activation highlighting morphological changes. (**F**) Western blot analysis and (**G**) gene expression analysis using quantitative polymerase chain reaction (qPCR) for α-SMA and ITGA5 in hPSCs with or without TGF-β activation. Data represent means ± SEM from at least three independent experiments. *$P < 0.05$ and ***$P < 0.001$.

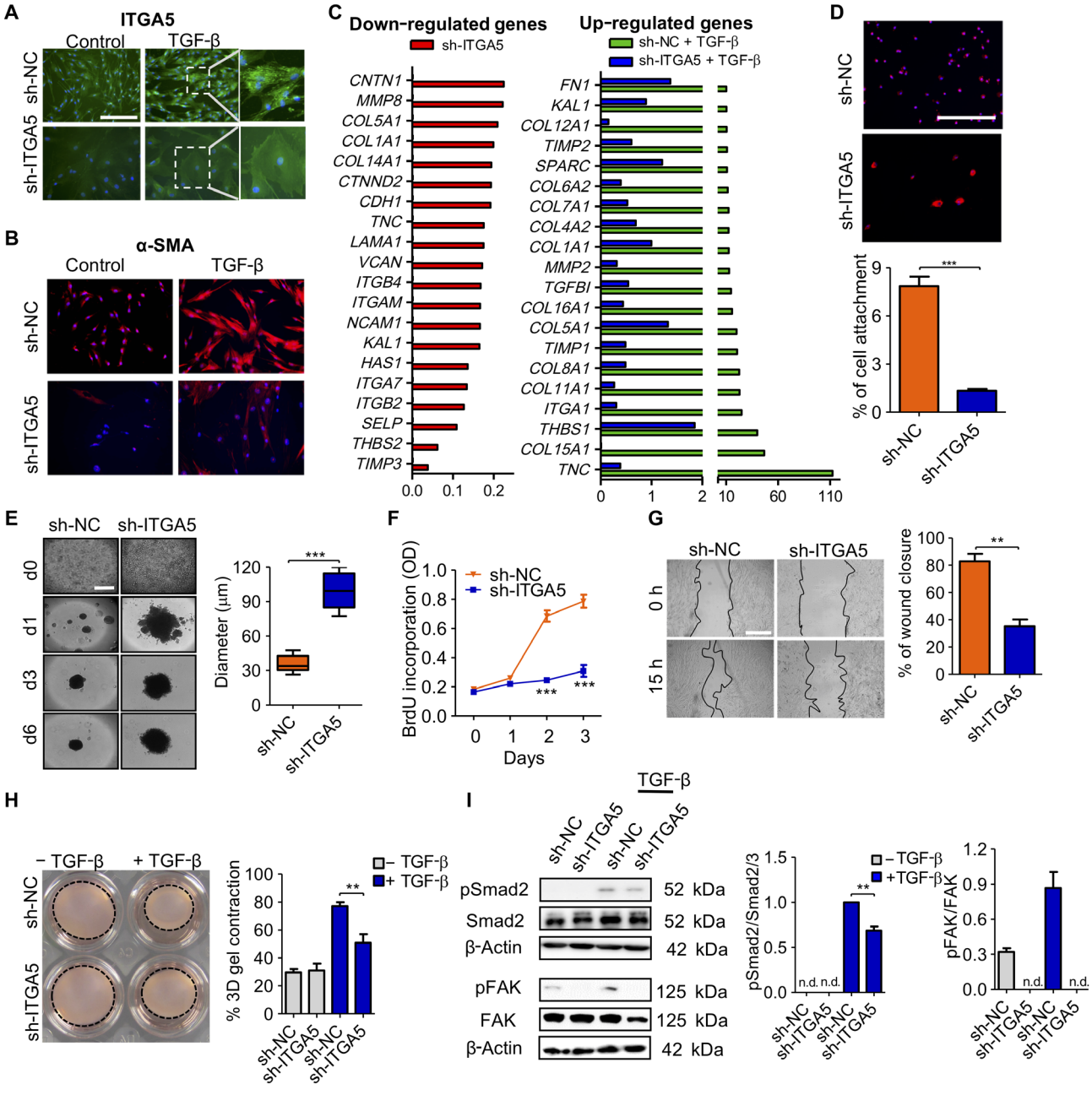

Fig. 2. ITGA5 knockdown attenuates hPSC activation, differentiation, and functions. Immunofluorescence staining showing ITGA5 (**A**) and α-SMA (**B**) expression in hPSCs after ITGA5 knockdown (sh-ITGA5) compared to NC (sh-NC) hPSCs with or without TGF-β activation. (**C**) Differential gene expression of adhesion molecules and ECM using human ECM RT^2 Profiler PCR Array in sh-ITGA5 with or without TGF-β activation. Left graph: sh-ITGA5 data are relative to sh-NC (set at 1.0) showing top 20 down-regulated genes after ITGA5 knockdown. Right graph: sh-NC + TGF-β data are relative to sh-NC hPSCs, while sh-ITGA5 + TGF-β data are relative to sh-ITGA5 hPSCs, showing the most induced genes after TGF-β activation, which are not induced after ITGA5 knockdown. (**D**) Cell adhesion assay shows that ITGA5 knockdown in hPSCs (sh-ITGA5) reduced cell attachment to the coated FN at $t = 30$ min compared to control hPSCs (sh-NC). Scale bar, 100 μm. (**E**) Spheroid formation assay shows that sh-ITGA5 hPSCs do not form compact spheroid due to lowered cell-to-cell attachment. (**F**) BrdU enzyme-linked immunosorbent assay (ELISA) shows that sh-ITGA5 hPSCs had a reduced cell proliferation compared to sh-NC assessed for 3 days. (**G**) Representative microscopic images of wound closure assay and quantitative analyses at $t = 15$ hours shows that sh-ITGA5 hPSC had a reduced migration ability. (**H**) Representative images from 3D collagen gel contractility assay show that TGF-β–induced contractility was inhibited in sh-ITGA5 hPSCs after 96 hours. (**I**) Western blot analysis (bands and quantitative analysis) shows that sh-ITGA5 hPSCs had a reduced TGF-β–induced pSmad2 and pFAK signaling in comparison to sh-NC hPSCs. The pSmad2/Smad2 ratio was analyzed at $t = 30$ min, while the pFAK-Y397/FAK ratio was analyzed at $t = 48$ hours. Densitometry analyses were performed using ImageJ software. Data represent means ± SEM from at least three independent experiments. *$P < 0.05$, **$P < 0.01$, and ***$P < 0.001$. Scale bar, 200 μm. n.d., not determined.

a half LIM domain protein 3) and PXN, and downstream genes, i.e., Rho family proteins CDC42, RAC1, and RHOA (fig. S1C). The expression levels of these genes, either without or with TGF-β activation, were significantly reduced in ITGA5 knockdown hPSCs (fig. S1C). These findings demonstrate that ITGA5 controls TGF-β–induced activation of PSCs via pSmad2 and pFAK signaling pathways.

ITGA5 knockdown abolishes PSC-induced protumorigenic effect in vitro and in vivo

Differentiated PSCs or CAFs secrete growth factors and cytokines that stimulate tumor cells for their proliferation and migration, as depicted in Fig. 3A. To mimic this process, we collected conditioned media from sh-ITGA5 and sh-NC hPSCs with or without TGF-β activation. In our previous study, we have shown that PANC-1 tumor cells treated with conditioned media collected from TGF-β–activated hPSCs displayed higher tumor cell growth (*10*). In this study, we found the similar paracrine effect of the TGF-β–activated hPSCs on PANC-1 cells (Fig. 3B). Conditioned media obtained from TGF-β–activated sh-ITGA5 hPSCs did not induce the growth of tumor cells (Fig. 3B). Likewise, we evaluated the effect of sh-ITGA5 and sh-NC hPSCs conditioned media on the migration of PANC-1 tumor cells using a transwell migration assay. Notably, tumor cells with sh-ITGA5 hPSCs conditioned media showed lower migration than those treated with the sh-NC hPSCs conditioned media (Fig. 3C). The conditioned media from TGF-β–activated sh-ITGA5 hPSCs did not induce the migration of PANC-1. These data suggest that knockdown of ITGA5 in hPSCs inhibits the paracrine interactions between PSCs and pancreatic cancer cells. To investigate whether knockdown of ITGA5 in hPSCs retards their protumorigenic effects in vivo, we established a co-injection tumor model in immunodeficient severe combined immunodeficient (SCID) mice. Consistent with previous reports (*24*, *25*), tumors derived from co-injection of PANC-1 and hPSCs showed a significantly increased tumor growth compared to tumors with PANC-1 cells alone (Fig. 3D). Furthermore, immunohistological examination revealed that PANC-1 + hPSC tumors were highly fibrotic, as indicated by overexpression of α-SMA and collagen I,

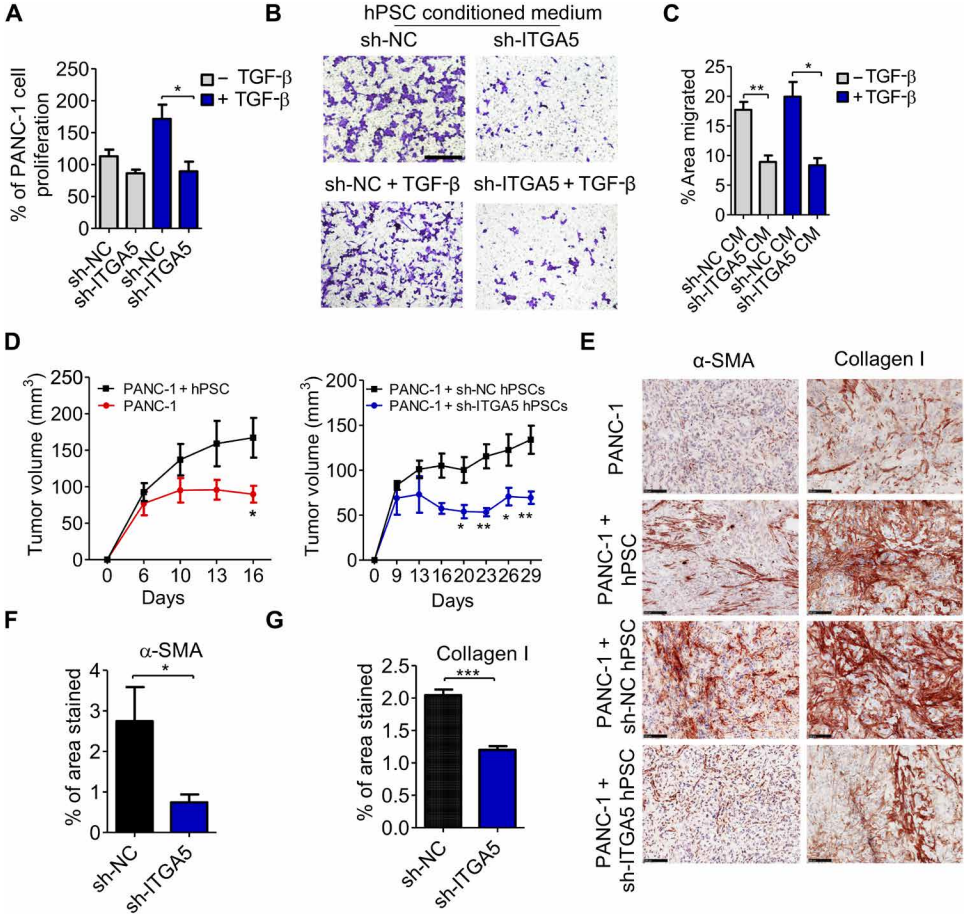

Fig. 3. ITGA5 knockdown abolishes PSC-induced protumorigenic effects. (**A**) Schematic representation of the paracrine effect of hPSCs on tumor cells. (**B**) PANC-1 tumor cell growth after 72 hours of incubation with conditioned medium obtained from sh-NC or sh-ITGA5 hPSCs activated either with or without TGF-β1. Cell growth was determined using alamarBlue assay performed at $t = 0$ hours and $t = 72$ hours and presented as % of $t = 0$ hours. Scale bar, 100 μm. (**C**) Effect of hPSC on PANC-1 migration. Representative images from transwell insert assay showing the migration of PANC-1 after incubation for 16 hours with conditioned medium (CM) from either sh-NC or sh-ITGA5 hPSCs with or without TGF-β. Data show that TGF-β–activated hPSCs did not induce PANC-1 migration, while there was a reduced migration of PANC-1 with sh-ITGA5 conditioned medium compared to sh-NC conditioned medium. Data represent means ± SEM from at least three independent experiments. *$P < 0.001$. (**D**) Tumor growth curves comparing the tumor growth of PANC-1 versus PANC-1 + hPSCs (left graph) and PANC-1 + sh-NC hPSCs versus PANC-1 + sh-ITGA5 hPSCs (right graph). Data represent means + SEM, *$P < 0.05$, **$P < 0.01$. (**E**) Representative microscopic pictures of immunohistochemical staining for α-SMA and collagen I in tumors. Scale bar, 100 μm. (**F** and **G**) Quantitation of α-SMA and collagen I staining, respectively. Data represents means + SEM. *$P < 0.05$, ***$P < 0.001$.

in comparison with PANC-1 tumors (Fig. 3E). Subsequently, we induced tumors by co-injecting PANC-1 with hPSCs, stably transfected with either sh-NC or sh-ITGA5 lentiviral plasmids. The sh-ITGA5 hPSCs had a stable knockdown of 55%. As shown in Fig. 3D, we found that PANC-1 + hPSC (sh-ITGA5) tumors had a significantly slower tumor growth than PANC-1 + hPSCs (sh-NC) tumors (Fig. 3D). Furthermore, tumors with ITGA5 knockdown hPSCs showed significantly less fibrosis area compared to tumors with normal hPSCs, as shown by immunohistochemical staining of α-SMA and collagen I (Fig. 3, E to G). These findings suggest that ITGA5 in hPSCs plays a key role in inducing its protumorigenic actions in vivo.

Novel ITGA5-antagonizing peptidomimetic (AV3) inhibits hPSC activation

To develop a therapeutic peptidomimetic specifically against ITGA5, overlapping sequences (12 amino acids long with 8–amino acid overlaps) from human FN-III domains 9 and 10 were synthesized and displayed on a cellular membrane. Domains 9 and 10 of FN-III are reported to be responsible for binding to the α5β1 receptor, as shown by the docking experiments elsewhere (*26*). With the interaction studies between the identified sequences and α5β1 receptor, we found that the sequence "TTVRYYRITYGE" strongly bound to the receptor, and by sequence reduction studies, we reached the sequence RYYRITY (named here as AV3) as the minimal sequence (Fig. 4A), responsible for the binding to α5β1. To demonstrate the specificity of AV3 to α5 subunit, we already showed binding to ITGA5 knockdown PSCs. In addition, during the screening process, we also performed receptor interaction studies of peptidomimetic with α4β1 and found that AV3 specifically bound to α5β1 receptor but not to other integrin receptor. As β1 was a common subunit in these receptors and AV3 only bound to α5β1, we expect that AV3 bound selectively to the α5 unit. The binding studies with peptidomimetic AV3 conjugated with 5-FAM fluorescent dye via a poly(ethylene glycol) (PEG) linker at the C-terminal site [AV3-PEG(6)-K-FAM] showed strong binding to TGF-β–activated hPSCs, as shown by fluorescence microscopy (Fig. 4B). The increase in binding was in line with the increased ITGA5 expression after TGF-β activation (Fig. 1, E to G). In sh-ITGA5 hPSCs, the binding was strongly reduced, showing the specific binding of AV3 to the ITGA5 receptor (Fig. 4B). Furthermore, we investigated the effect of AV3 on the TGF-β–mediated activation of hPSCs. AV3 significantly reduced the expression levels of differentiation marker α-SMA and collagen I, as shown by immunocytochemical staining and Western blot analysis (Fig. 4, C and D). We also examined whether AV3 could inactivate already activated CAFs isolated from patients and observed a clear inactivation of the primary pancreatic CAFs, as shown by immunocytochemical staining for α-SMA and collagen I (fig. S2A). In contrast, scrambled AV3 did not show any inhibitory effects in these analyses. Furthermore, we found that AV3 also inhibited the TGF-β–induced contractility of hPSCs in 3D collagen gel (Fig. 4E), which is in line with the ITGA5 knockdown data (Fig. 2H). Because AV3 inhibited the TGF-β–mediated effects, we were interested in understanding the mechanism of action of AV3. In Fig. 2I, we showed that knockdown of ITGA5 in hPSCs resulted in the inhibition of TGF-β–induced pSmad2 and pFAK signaling. We found that treatment with AV3 significantly inhibited FAK phosphorylation (Fig. 4F), while it did not inhibit pSmad2 pathways (fig. S2B).

AV3 enhances the cytotoxic effect of gemcitabine in 3D heterospheroids

PANC-1 or MIA PaCa-2 cells were cocultured with hPSCs in a 1:1 ratio to form 3D heterospheroids. To examine the AV3 inhibitory effects on 3D heterospheroid growth, we treated the established heterospheroids on days 3 and 6 with either AV3, gemcitabine, or cotreatment with AV3 and gemcitabine and monitored their growth until day 9. Spheroids consist of hPSCs and either PANC-1 or MIA PaCa-2 cells showed an increase in size over the culture period (Fig. 4, G and H). In PANC-1 heterospheroids, a small but significant difference in the spheroid volume was observed in the AV3-treated group compared to the vehicle group, but no difference was seen in MIA PaCa-2 heterospheroids. In both heterospheroids, we observed that cotreatment with AV3 and gemcitabine led to a smaller spheroid volume compared to spheroids treated with only gemcitabine or AV3 (Fig. 4, G and H). In addition, to determine the spheroid viability by AV3 and/or gemcitabine, we examined cell viability using adenosine triphosphate (ATP) analysis. PANC-1 and MIA PaCa-2 heterospheroids showed a substantial reduction in cell viability, which was much higher than AV3 or gemcitabine alone. To demonstrate that AV3 enhanced antitumor effects due to inhibition of stroma, we also examined the effect of AV3 in monospheroids composed of only PANC-1 or MIA PaCa-2 tumor cells. We found that treatment with gemcitabine reduced the spheroid volume but that cotreatment with AV3 did not show any additional benefit (fig. S2C). These data indicate that the effect of AV3 on the increase of antitumor effect of gemcitabine is due to inhibition of stroma.

AV3 reduces desmoplasia, enhances tumor perfusion, and potentiates the efficacy of gemcitabine in vivo

As shown in Fig. 3D, we already demonstrated that co-injection of hPSCs with PANC-1 tumor cells stimulated tumor growth by inducing fibrosis and that knockdown of ITGA5 in hPSCs restricted this enhancement of the tumor growth. In one of the preliminary co-injection (hPSCs + PANC-1) tumor models, we confirmed that our AV3 peptidomimetic is able to inhibit the hPSC-induced fibrosis and the tumor growth after administering either intraperitoneal or local intratumoral injection (fig. S3, A and B). As expected, the scrambled peptidomimetic (sAV3) did not show any inhibitory effect. We found that the treated tumors had reduced ECM deposition and activated fibroblasts, as shown by immunostainings for collagen I and fibroblast activation markers such as desmin (fig. S3C). Furthermore, AV3 was well tolerated by the animals, as there was no change in the body weight and organ weight after multiple treatments (fig. S3, C and D). Having seen the antifibrotic effect of AV3 in vivo, we extended our investigations in co-injection (hPSCs with PANC-1 or MIA PaCa-2) tumor models. In the PANC-1 + hPSC tumor model, treatment with AV3 alone showed moderate effects on tumor growth inhibition, but cotreatment with AV3 and gemcitabine reduced the tumor growth by 75% compared to the vehicle group and also significantly more than gemcitabine alone (Fig. 5A). Moreover, these results were also confirmed in the isolated tumor size and weight at the end of the experiments (Fig. 5, B and C). We observed no toxicity of AV3 on body weight or organ (liver and lungs) weights (fig. S4, A and B). Furthermore, we examined the antifibrotic effects in PANC-1 tumors and found that the treatment with AV3 alone or combined treatment reduced the expression of collagen I (Fig. 5E). Moreover, we found that the blood vessel lumens in AV3-treated tumors were expanded and opened up, as shown in Fig. 5E (see arrows). In the

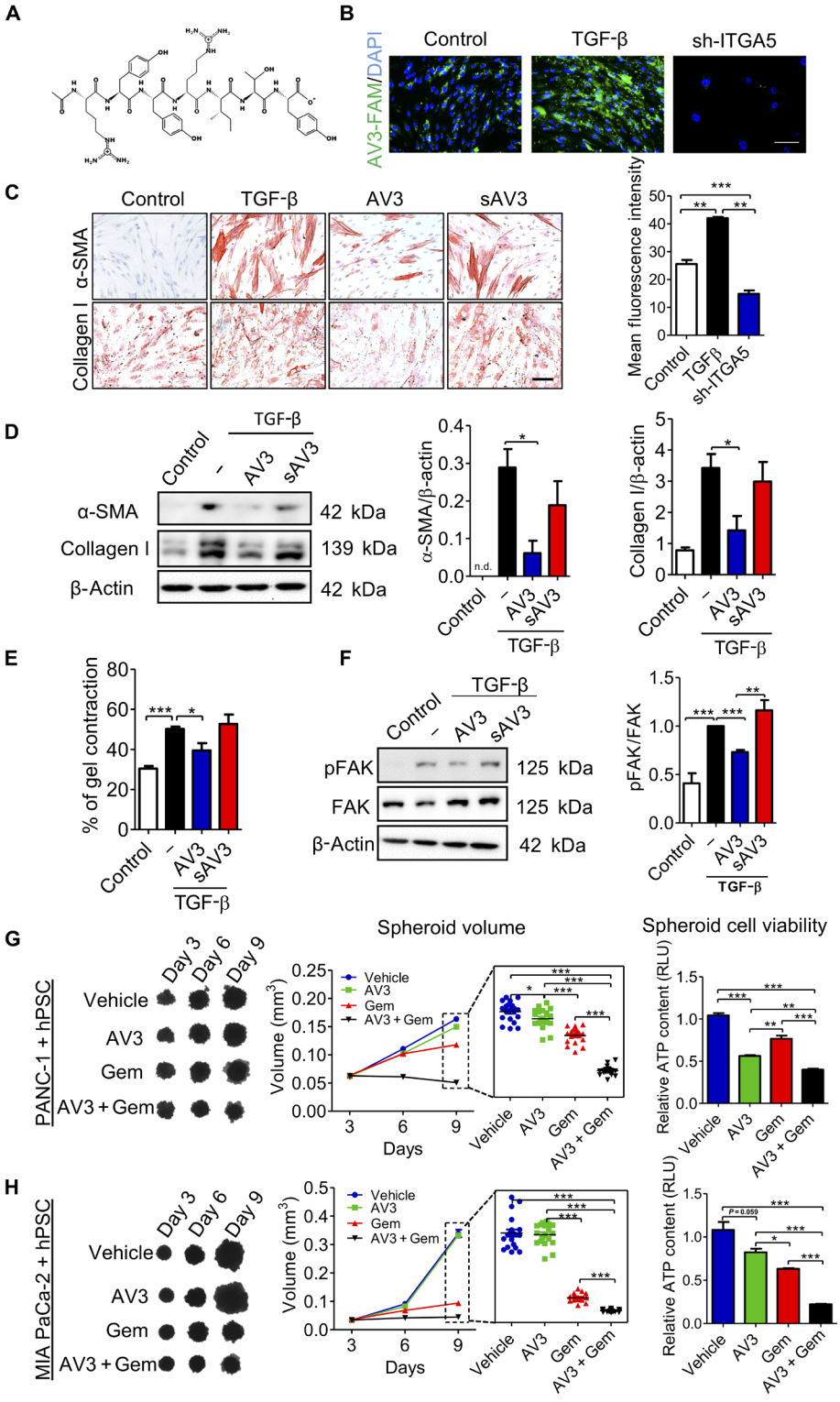

Fig. 4. A novel peptidomimetic (AV3) against ITGA5. (**A**) Chemical structure of AV3 peptidomimetic. (**B**) Binding of AV3-FAM in control hPSCs, TGF-β–activated hPSCs, and sh-ITGA5 hPSCs, as shown in the representative microscopic fluorescent images and quantitative analysis from flow cytometry. (**C** and **D**) Immunocytochemical staining and Western blot analyses show that AV3 inhibits α-SMA and collagen I expression levels in hPSCs, whereas scrambled (s)AV3 shows no inhibitory effects. (**E**) Bar graph showing the results from the collagen gel assay in which AV3 inhibits TGF-β–induced collagen gel contractility after 72 hours. (**F**) Western blot analyses showing the expression levels of pFAK, FAK, and β-actin in hPSCs following AV3 treatment of TGF-β–activated hPSCs for 8 hours. (**G**) Representative images of PANC-1 + hPSC (A) and MIA PaCa-2 + hPSC (**H**) heterospheroids. The graph shows the spheroid volume and cell viability after the treatment with AV3 and cotreatment with AV3 and gemcitabine compared to either vehicle- or gemcitabine-treated spheroids. Data represent means ± SEM from at least three independent experiments. **P* < 0.05, ***P* < 0.01, and ****P* < 0.001.

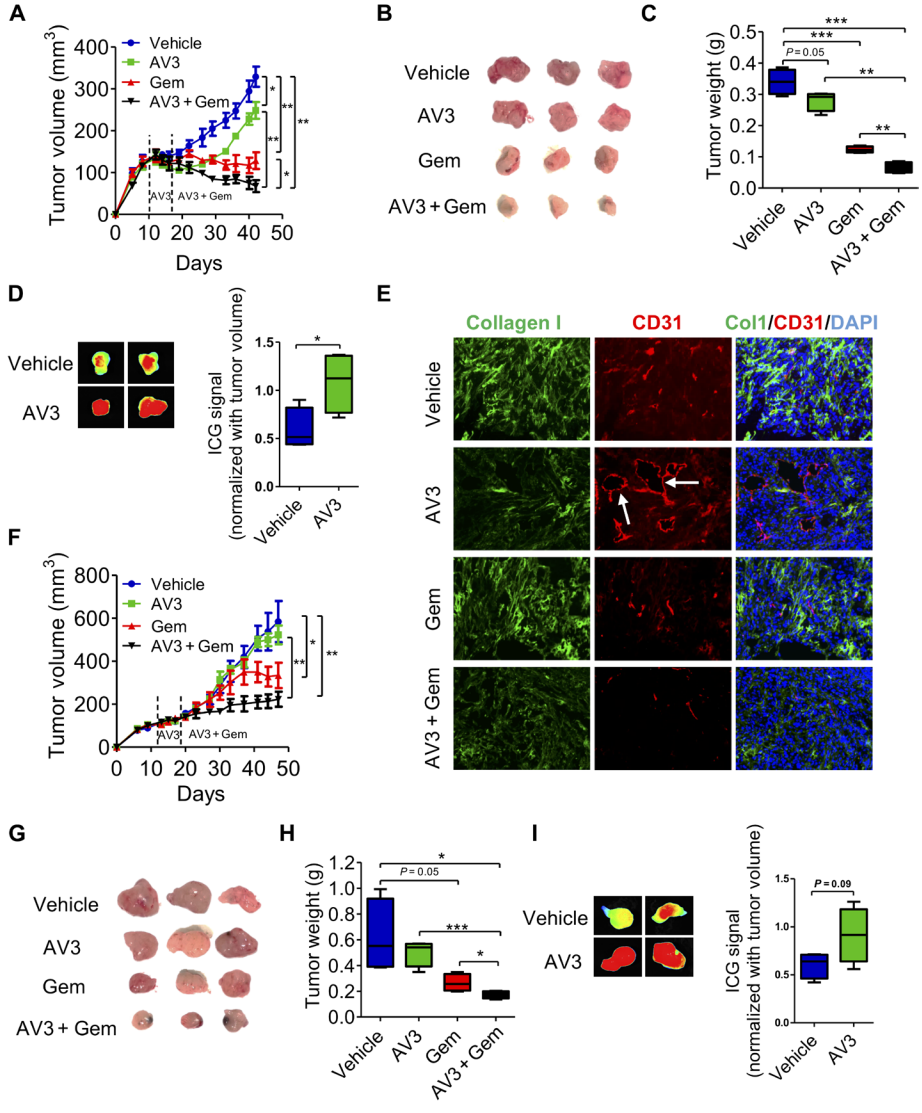

Fig. 5. AV3 reduces PSC-induced pancreatic tumor growth and potentiates the effect of gemcitabine in co-injection tumor models in mice. The dataset A–E belongs to PANC-1 + hPSCs, while the dataset F–I belongs to MIA PaCa-2 + hPSCs. (**A** and **F**) Tumor growth curve of PANC-1 + hPSC and MIA PaCa + hPSC tumors after the treatment with vehicle, AV3, gemcitabine (Gem), or AV3 + Gem. AV3 was administered at the dose of 20 mg/kg, intraperitoneally, three times per week for only the first week, followed by biweekly, while gemcitabine was administered at the dose of 50 mg/kg, intraperitoneally, biweekly (after the second dotted line). Data are represented as means ± SEM. $n = 4$ mice per group. $^{*}P < 0.05$, $^{**}P < 0.01$, and $^{***}P < 0.001$. (**B** and **G**) Images of the isolated PANC-1 + hPSC and MIA PaCa + hPSC tumors and (**C** and **H**) tumor weights of the isolated PANC-1 + hPSC and MIA PaCa + hPSC tumors at the end of the experiment. (**D** and **I**) Optical imaging showing the effect of AV3 on the accumulation of ICG dye in PANC-1 + hPSC and MIA PaCa + hPSC tumors. Mice were injected with ICG dye via tail vein at the dose of 5 mg/kg. After 24 hours of the injection, isolated tumors were imaged using a near-infrared (NIR) animal imager. The degree of ICG fluorescence signal was quantified. $n = 4$ mice per group. Data represent means ± SEM. $^{*}P < 0.05$. (**E**) Microscopic images of immunofluorescence staining of collagen I show that the treatment with AV3 alone or combined with gemcitabine reduced the expression of collagen I. Blood vessel lumens in AV3-treated tumors were decompressed, as shown in (E) (see arrows).

MIA PaCa-2 + hPSC co-injection model, treatment with AV3 showed no effect on the tumor growth but cotreatment with gemcitabine resulted in the enhanced effects on the tumor growth inhibition (Fig. 5F). These effects became more obvious in the images and weights of the isolated tumors (Fig. 5, G and H). To confirm the effect of AV3 on the tumor perfusion, we performed tumor distribution of the indocyanine green (ICG) dye using near-infrared (NIR) imaging and found that treatment with AV3 significantly enhanced the tumor perfusion, as can be seen with higher accumulation of ICG dye in AV3-treated tumors in both tumor models (Fig. 5, D and I). To demonstrate that the effects of AV3 were due to its accumulation in tumor, we labeled AV3 with IR680 NIR dye and injected intravenously into PANC-1 + hPSC tumor-bearing mice with/without excess of unlabeled AV3. We found that AV3-IR680 accumulated into the tumors, and competition with unlabeled AV3 significantly reduced its accumulation (fig. S4C). These data indicate that AV3 accumulated into tumors and elicited its effects.

AV3 potentiates the efficacy of gemcitabine in the PDX model

Having seen the anti-stromal effect and potentiation of the effect of chemotherapy with AV3, we investigated the effect of AV3 in a PDX

pancreatic tumor model. To retain the closest pancreatic morphological features, we used an early passage of PDX tumor, as shown in Fig. 6A. A small piece of the pancreatic tumor was isolated from a patient and grown to passage 2 (P2), followed by implanting into the flank of nonobese diabetic (NOD)/SCID mice. To confirm that the used tumor had abundant stroma and expressed ITGA5, we examined the P0 tumor (tumor from patient 193) for the expression of ITGA5, α-SMA, and collagen I immunohistochemically and found high expression levels of these markers (fig. S5A). This early-passage PDX mouse model showed maintenance of tumor nests and compressed blood vessels, similar to human tumor (fig. S5B). As expected, treatment with gemcitabine reduced the growth of the PDX significantly, but cotreatment with AV3 reduced the tumor growth markedly, as can be seen from the tumor growth curves and isolated tumors (Fig. 6, B and C). Furthermore, these results were confirmed by the weights of the isolated tumors at the end of the experiment (Fig. 6D). Similar to co-injection tumor models, treatment with AV3 showed enhanced tumor perfusion in most animals, which was shown by higher accumulation of ICG dye in AV3-treated tumors (Fig. 6E). Furthermore, we found that the treatment with AV3 alone or combined treatment reduced the expression of collagen I (Fig. 6F), which was related to the reduction of CAF activation, as shown by α-SMA immunostaining (fig. S5C). Notably, gemcitabine alone did not show these effects. In line with co-injection tumor models, we found that the blood vessel lumens in AV3-treated tumors were decompressed, as shown in Fig. 6F (see arrows). However, with combination therapy, the lumen decompression was not seen, which might be due to cytotoxicity of gemcitabine to endothelial cells and pericytes. These data suggest that the reduction in fibrosis supported decompression of blood vessels and thereby induced delivery of gemcitabine into tumors and the antitumor effects. We also show that treatment with AV3 did not show any toxic effects in either of the models, as can be seen with the body, liver, and lung weights (fig. S5D). Furthermore, we investigated whether AV3 could inhibit phosphorylation of FAK in AV3-treated tumors compared to vehicle-treated tumors. We found a clear reduction of pFAK in some animals, as shown by Western blot analysis (fig. S5E). However, we also observed a reduction of total FAK, which might be due to the reduction of the total stroma after multiple treatments with AV3.

DISCUSSION

The abundant desmoplastic stroma reaction in pancreatic tumors has been recognized for inducing aggressive tumor growth, distant metastasis, and resistance to drug therapy and acting as a barrier to drug delivery (*27*). Targets within the tumor stroma are therefore under scrutiny to improve prognosis by developing novel therapeutics aimed at hampering its tumor-promoting function. In the present study, we highlight ITGA5 as a key target in tumor stroma, showing its significance in the prognosis of pancreatic cancer. Our ITGA5

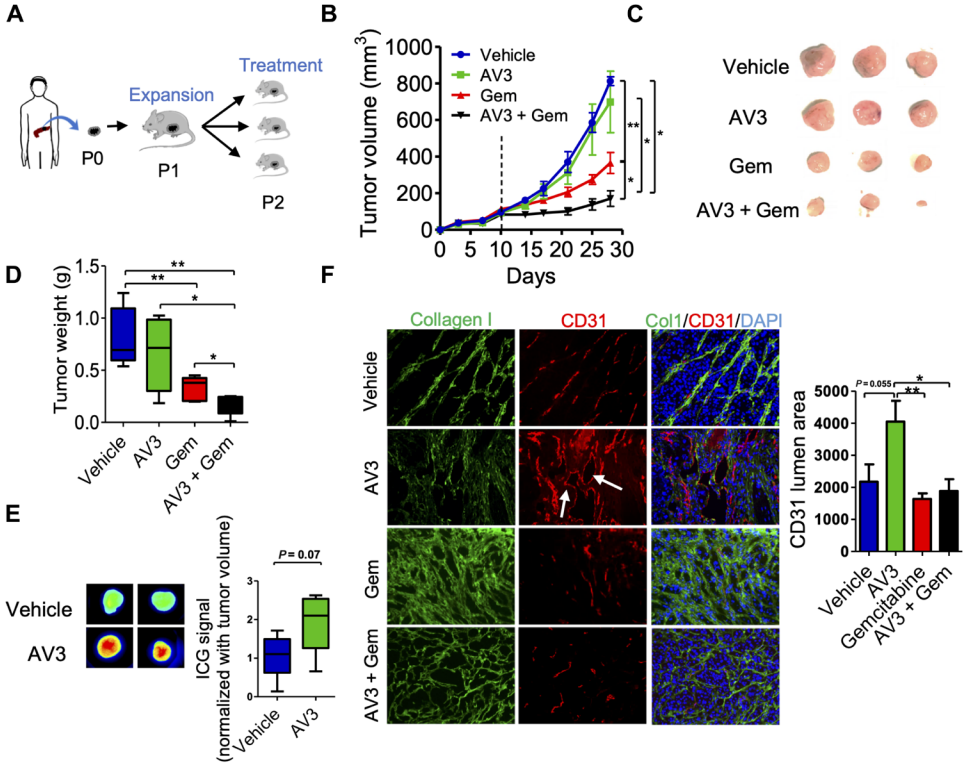

Fig. 6. AV3 potentiates the effect of gemcitabine in the PDX model in mice. (**A**) Schematic representation of the generation of the human pancreatic PDX tumor model. (**B**) Tumor growth curves in the PDX model after the treatment with vehicle, AV3 (20 mg/kg, intraperitoneally, twice a week), gemcitabine, or AV3 + Gem. The doses of AV3 and Gem were 20 and 50 mg/kg, respectively, intraperitoneally, biweekly, starting at day 0. Data represent means ± SEM. $n = 5$ mice per group. *$P < 0.05$ and **$P < 0.01$. (**C**) Images of the isolated tumors and (**D**) tumor weights at the end of the experiment. (**E**) NIR imaging showing the accumulation of ICG dye in tumors treated with either vehicle or AV3. The degree of ICG fluorescence signal was quantified. $n = 5$ mice per group. Data represent means ± SEM. (**F**) Microscopic pictures of immunohistochemical staining of collagen I and CD31, and CD31 lumen size quantitation. Data represent means ± SEM. *$P < 0.05$ and **$P < 0.01$.

knockdown studies showed that ITGA5 is crucial for the maintenance of the PSC phenotype and controls TGF-β–mediated activation through at least FAK and Smad2 pathways. Furthermore, knockdown of ITGA5 inhibited PSC-induced tumor cell growth and migration in vitro and PSC-driven tumor growth in vivo. A novel ITGA5 antagonistic peptidomimetic (AV3) was developed, which showed inhibition of hPSCs via the TGF-β/ITGA5/FAK pathway. In 3D heterospheroid models, AV3 enhanced the effect of gemcitabine. In vivo, AV3 reduced desmoplasia in three different tumor models (two stroma-rich co-injection xenograft models and PDX tumor model). The combination of AV3 to gemcitabine strongly enhanced its antitumor effects by reducing fibrosis, allowing decompression of blood vessels and improving access to tumor cells.

Integrins are highly up-regulated on the membrane of myofibroblasts, being the main producers of ECM molecules (*16*, *19*, *22*). The role of many integrin receptors in myofibroblasts has been reported to inhibit fibrosis in multiple organs such as the liver, lung, and kidney (*16*). ITGA5, a subunit of the FN receptor, is reportedly overexpressed in activated fibroblasts in fibrosis and cancer, as well as in tumor epithelial cells undergoing epithelial-mesenchymal transition (*18*, *28*, *29*). In the present study, overexpression of ITGA5 was observed in stromal CAFs in clinical samples of pancreatic cancer, and a very weak expression in malignant cells, confirming the specificity of ITGA5 for CAFs. In literature, high expression levels of CAF markers such as α-SMA and PDGFβR in the pancreatic tumor have been shown to be associated with poor prognosis (*30*, *31*). In line with these data, we identify ITGA5 as a novel stromal prognostic marker, as its high expression was independently associated with poor OS.

PSCs are regarded as the main source of CAFs (*7*, *9*), and upon activation with TGF-β, they acquire the myofibroblastic CAF phenotype, as shown earlier by us and others (*10*, *20*, *32*). TGF-β–mediated activation of hPSCs in vitro resulted in stretched and elongated α-SMA–expressing myofibroblasts, which overexpressed ITGA5 compared to non-activated cells. Notably, non-activated hPSCs were α-SMA negative but α-SMA positive for ITGA5. Knockdown of ITGA5 using shRNA, as shown in this study, led to the reprogramming of hPSCs inhibiting TGF-β–induced differentiation into myofibroblasts and ECM production. As shown using gene array (Fig. 2C), most of the TGF-β–induced genes in hPSCs were inhibited in ITGA5 knockdown (sh-ITGA5) hPSCs. Furthermore, ITGA5 knockdown hPSCs became flattened due to the loss of stress filaments and had reduced cell-to-cell adhesion, migration, proliferation, and contractile properties. These results can be explained as integrins are responsible for maintaining cell phenotype such as adhesion, migration, contraction, and proliferation (*15*).

Besides the change in the PSC phenotype, knockdown of ITGA5 also inhibited TGF-β–induced activation of hPSCs. In literature, integrins have been reported to interact with several growth factor receptors, including PDGFR-β, c-Met, vascular endothelial growth factor receptor (VEGFR), epidermal growth factor receptor (EGFR), and TGF-β receptors (*33*). On the one hand, TGF-β1 is shown to induce the expression of α5β1 and activate FAK signaling due to ligation and clustering of integrins (*34*). On the other hand, α5β1 integrin is also shown to modulate TGF-β1/Smad pathways directly or indirectly via different mechanisms (*22*, *23*). In line with these data, we here show that TGF-β1 activates not only its own signaling pathways (pSmad2) but also the ITGA5-mediated pFAK signaling pathway. ITGA5 knockdown in hPSCs inhibited TGF-β–mediated pSmad2 and pFAK pathways, which at least partly explains the mechanisms behind the inhibition of TGF-β–induced hPSC activation. Furthermore, inhibition of the gene expression of direct ITGA5-related signaling molecules such as FLH3 and paxillin, as well as downstream factors (CDC42, RAC1, and RHOA) in ITGA5 knockdown hPSCs, explains the inhibitory effects on migration, proliferation, adhesion, and contraction (fig. S1C).

Our data show inhibition of hPSC-mediated paracrine effect on tumor cell growth and migration after ITGA5 knockdown, as shown in Fig. 3. These findings corroborate results of a recent study showing that inhibition of kindlin-2, an integrin-activating focal adhesion protein, leads to inhibition of PSC-induced tumor cell activation (*35*). The hPSC-induced fibrosis and tumor-promoting effects were confirmed in vivo in a co-injection tumor model, as shown by induced fibrosis markers (α-SMA and collagen I) and tumor progression. These findings are consistent with previous studies showing PSC-induced pancreatic tumor growth (*9*, *24*). In line with our in vitro data, ITGA5 knockdown in hPSCs led to reduced fibrosis in tumors, which resulted in a reduced tumor progression. The reduced tumor progression was not due to the death of hPSCs, and we confirmed the presence of activated hPSCs using α-SMA immunostaining.

Furthermore, our novel AV3 peptidomimetic robustly showed specific binding to the ITGA5 receptor, resulting in reduced TGF-β–mediated activation of hPSCs by inhibiting the FAK pathway. We revealed that activation of TGF-β induced the phosphorylation of FAK, most likely by up-regulating the ITGA5 receptor and its ligand FN expression levels (Figs. 1G and 2C), given that FAK is the downstream signaling pathway of ITGA5/FN interaction. Blocking of ITGA5 with AV3 inhibited the activation of the FAK pathway, as observed with ITGA5 knockdown studies in Fig. 2I, and thereby inhibited pFAK-induced fibrotic factors such as α-SMA and collagen in hPSCs. In contrast to ITGA5 knockdown study, AV3 did not inhibit pSmad2, which might be due to differences between acute receptor blockade and the permanent receptor removal due to stable knockdown. Fundamentally, this pathway is very different compared to an inhibitor for the TGF-β receptor or FAK pathway. Direct inhibition of TGF-β is associated with severe side effects such as cardiotoxicity (*36*). Because the FAK pathway is a downstream pathway of many receptors, inhibition of it will block several pathways. However, in this study, we emphasize the role of the TGF-β/ITGA5/FAK pathway, which is rather unique in controlling PSC differentiation and ECM production via TGF-β. We show that, by inhibiting ITGA5 using AV3, we can inhibit this TGF-β–mediated ITGA5/FAK pathway and thereby fibrotic genes.

Recent advances have triggered an interest in spheroid culture as an in vitro model for drug screening (*11*). Here, we investigated the effect of AV3 and gemcitabine in 3D heterospheroids formed from tumor cells (PANC-1 or MIA PaCa-2) and hPSCs. Treatment with AV3 and gemcitabine reduced the spheroid area over time, and the combination treatment resulted in higher efficacy than the monotreatment. In 3D monospheroids (either PANC-1 or MIA PaCa-2), we did not observe the enhanced effect of AV3 on the effect of gemcitabine compared to gemcitabine treatment alone (fig. S2C).

In vivo, the specific targeting of AV3 to tumors was confirmed by the specific tumor accumulation of IR680-labeled AV3, as shown by NIR imaging in PANC-1 + hPSC tumors (fig. S4C). Treatment with AV3 either systemically (intraperitoneally) or locally (intratumorally) reduced the tumor growth due to the reduction of desmoplasia, which is in agreement with the sh-ITGA5 hPSC in vivo data. In line with our in vitro 3D heterospheroid data, cotreatment

with AV3 significantly enhanced the anticancer effect of gemcitabine in both co-injection and PDX tumor models. We observed the direct inhibitory effect of AV3 on the tumor growth in the co-injection model (fig. S3 and Fig. 5A), which is likely due to a reduction in PSC activation and inhibition of PSC-induced tumor cell growth. However, in MIA PaCa-2 + hPSC and PDX models, we did not observe any direct effect of AV3 on the tumor growth, despite the reduction in fibrosis (Figs. 5E and 6F). Therefore, these data indicate that AV3 did not inhibit PSC-induced tumor proliferation in vivo but inhibited PSC-induced fibrosis and thereby enhanced the efficacy of gemcitabine. Furthermore, we found reduction of both pFAK and FAK levels in some tumors treated with AV3 compared to vehicle group (fig. S5E). The limited effect of FAK might be due to a long gap of 48 hours between tumor isolation and the last dose of AV3. Nevertheless, these data indicate that the in vivo effect of AV3 on pFAK is in line with in vitro studies. Furthermore, we showed that the treatment with AV3 alone shows the decompression of blood vessels. However, with AV3 and gemcitabine treatment, no decompression was seen, probably due to cytotoxicity of gemcitabine to endothelial cells and pericytes. Histologically, we showed that AV3 consistently reduced collagen I deposition in both co-injection tumor models and the PDX tumor model and allowed blood vessels to decompress, as could be seen with endothelial cell marker CD31 immunostaining. The reduction in ECM after the treatment with AV3 led to the decompression of tumor vasculature, which was seen in AV3-treated tumors but not in the cotreatment (AV3 and gemcitabine) group. As the tumor growth after the cotreatment with AV3 and gemcitabine reduced by 80% due to toxicity on tumor cells but likely on the proliferation of endothelial cells, these tumors do not represent the effect of AV3 on the decompression of vasculature. Decompression of tumor vasculature allowed enhanced tumor perfusion in AV3-treated tumors, as confirmed with enhanced ICG tumor accumulation.

In conclusion, this study reveals ITGA5 as a novel prognostic and therapeutic target in pancreatic cancer with a strong impact on the regulation of PSC-induced desmoplasia in pancreatic cancer. In addition, it sheds new light on the importance of ITGA5 on the regulation of the TGF-β–mediated PSC activation. The new endogenous peptidomimetic AV3 against ITGA5 showed inhibition of TGF-β–mediated PSC activation in vitro and reduced desmoplasia in vivo. Furthermore, our data showed that treatment with AV3 enhanced the efficacy of gemcitabine in different co-injection tumor models and an early-passage PDX model. This enhancement was attributed to the reduction of desmoplasia (collagen deposition) caused by AV3 treatment. Together, this study provides compelling evidence that inhibition of ITGA5 using our novel peptidomimetic may improve the efficacy of chemotherapy in pancreatic cancer.

MATERIALS AND METHODS

Study design

This study was designed to show ITGA5 as a therapeutic target in PSCs and to assess the therapeutic potential of the novel peptidomimetic (AV3) in combination with chemotherapy in a PDX pancreatic tumor model. We investigated the prognostic value of ITGA5 in patients with PDAC, and the tissue samples were obtained during 2001 to 2012 from 137 patients with pancreatic adenocarcinoma. In vitro assays (qPCR, Western blot, immunocytochemistry, migration assay, and contraction assays) and in vivo xenograft tumor models (co-injection tumor model and PDX models) were used to investigate ITGA5 as a therapeutic target in PSCs and the efficacy of novel peptidomimetic AV3. Most of the findings were evaluated by more than one method, and experiments were repeated multiple times independently. In vivo experiments were randomized and partly blinded, and the number of samples was calculated using power test considering meaningful differences, % coefficient of variation within the experiment, and a minimum P value of 0.05. Cultured cells or PDX tissues were used for these animal models. All experiments were conducted under the international animal ethical guidelines, which were approved by the animal ethical committee of Utrecht University, The Netherlands.

Cells

hPSCs were purchased from ScienCell (Carlsbad, CA) and maintained in a special culture medium provided by the manufacturer, supplemented with 1% penicillin/streptomycin. The pancreatic cancer cell line (PANC-1) was obtained from the American Type Culture Collection (Rockville, MD) and cultured in Dulbecco's modified Eagle's medium (PAA, The Netherlands) supplemented with fetal bovine serum (FBS; 10%) and antibiotics (1% penicillin/streptomycin). To knock down ITGA5, hPSCs were transfected with custom-made lentiviral vector shRNA plasmids against ITGA5 (gene ID: 3678) under puromycin resistance (ATCGbio Life Technology Inc., Burnaby, Canada) using Lipofectamine 2000 transfection reagent (Thermo Fisher Scientific, Breda, The Netherlands).

Peptidomimetics

To select a peptidomimetic ligand against ITGA5, overlapping sequences (12 amino acids long with 8–amino acid overlaps) from human FN-III domains 9 and 10 were designed and displayed on a cellular membrane. Domains 9 and 10 of FN were chosen to design peptidomimetics, as these domains were reported to be responsible for binding to the α5β1 receptor, as shown by the docking experiments (*26*). The interaction studies were performed against human recombinant integrin α5β1 receptor (R&D Systems), the bound proteins were transferred to another membrane, and ITGA5 was detected with antibodies. AV3 (Arg-Tyr-Tyr-Arg-Ile-Thr-Tyr) and AV3-PEG6-5FAM (AV3-FAM) were custom-synthesized by China Peptide Co. Ltd. (Shanghai, China). The % purities were 98% for AV3 and 95% for AV3-PEG_6-5FAM, as assessed by reversed-phase high-performance liquid chromatography (HPLC, analytical). The products were stored at −20°C.

Patient material, immunohistochemistry, and scoring method

Collection of patient tissue material was approved by the institutional review board (IRB) of Leiden University Medical Centre (LUMC), Leiden, The Netherlands. Retrospectively collected, formalin-fixed, and paraffin-embedded tissue blocks were obtained from the archives of the Pathology Department for 137 patients with pancreatic adenocarcinoma, who underwent resection with curative intent during the period from 2001 to 2012 at the LUMC. Only patients with pancreatic adenocarcinoma were included in this study. None of the patients received chemotherapy and/or radiation before surgery. Clinicopathological data were collected from electronic hospital records. Differentiation grade was determined according to the guideline of the World Health Organization, and the TNM [T describes the size of the tumor and any spread of cancer into nearby tissue; N describes the spread of cancer to nearby lymph nodes; and M describes metastasis (spread of cancer to other parts of the body)] stage was defined according to the American Joint

Commission on Cancer criteria. All samples were nonidentifiable and used in accordance with the code for proper secondary use of human tissue as prescribed by the Foundation Federation of Dutch Medical Scientific Societies. The use of archived human tissues conformed to an informed protocol that had been reviewed and approved by the IRB of the LUMC, Leiden, The Netherlands.

Tissue microarrays (TMAs) were prepared to examine the expression of ITGA5 and α-SMA. For each patient, triplicate 2.0-mm cores were punched from areas with clear histopathological tumor representation [determined by hematoxylin and eosin (H&E) staining] from formalin-fixed paraffin-embedded tissue blocks of their primary tumor and transferred to a recipient TMA block using the TMA master (3DHISTECH, Budapest, Hungary). From each completed TMA, 5-μm sections were sliced and deparaffinized in xylene and then rehydrated in serially diluted alcohol solutions, followed by demineralized water. Endogenous peroxidase was blocked by incubation in 0.3% hydrogen peroxide in phosphate-buffered saline (PBS) for 20 min. Antigen retrieval was performed by heat induction at 95°C using citrate buffer (pH 6.0; Dako, Glostrup, Denmark). TMA sections were incubated overnight with antibodies against ITGA5 (HPA002642; Sigma-Aldrich) and α-SMA (PA5-16697; Thermo Fisher Scientific). NC samples were incubated with PBS instead of the primary antibodies. The slides were then incubated with Envision anti-rabbit (K4003; Dako) for 30 min at room temperature. After additional washing, immunohistochemical staining was visualized using 3,3′-diaminobenzidine tetrahydrochloride solution (Dako) for 5 to 10 min, resulting in brown color, and then counterstained with hematoxylin, dehydrated, and finally mounted in Pertex. All stained sections were scanned and viewed at 40% magnification using the Philips Ultra Fast Scanner 1.6 RA (Philips, Eindhoven, The Netherlands). The evaluation of the immunohistochemical stainings for ITGA5 and α-SMA on human TMA was performed in a blinded manner and independently by two qualified pathologists, and a good inter-observer concordance was found with Cohen's *K* score of 0.79.

The tumor/stroma ratio was determined on sections stained with H&E. The cutoff point for stromal high tumors was the presence of one tumor area with >50% tumor stroma. α-SMA staining was scored, according to the extent of stromal positivity, as positive when >50% of stroma stained positive. Stromal ITGA5 staining was categorized by multiplying the percentage of stained cells (P) by the intensity of staining (I). The percentage of stained cells is as follows: 0 (absence of stained cells), 1 (<25% stained cells), 2 (26 to 50% stained cells), and 3 (>50% stained cells). Staining intensities are as follows: 1 (mild), 2 (moderate), and 3 (intense). ITGA5 was considered to be positive when the final score (P × I) was >4. A double immunofluorescence staining was performed for α-SMA (green) and ITGA5 (red), and only green colored cells were considered α-SMA$^+$ only cells and red colored cells were ITGA5$^+$ only cells, while yellow colored cells were considered double-positive cells.

RNA isolation, reverse transcription, and qPCR

sh-NC or sh-ITGA5 hPSCs were lysed with lysis buffer for total RNA. RNA isolation, complementary DNA (cDNA), and qPCR were performed as described previously (*10*). The details of the primers are provided in table S3.

Western blot analyses and immunofluorescence staining

Cells were lysed with SDS-lysis buffer, and lysate was loaded on precasted tris-glycine (4 to 20% or 10%) gel (Thermo Fisher Scientific, Breda, The Netherlands) and transferred onto polyvinylidene difluoride (PVDF) membranes (Thermo Fisher Scientific). The blots were probed with the primary antibodies at different dilutions and were incubated overnight at 4°C, followed by incubation at room temperature for 1 hour with species-specific horseradish peroxidase–conjugated secondary antibodies. The details of the primary and secondary antibodies are provided in table S4. The proteins were detected using the Pierce ECL Plus Western Blotting Substrate Kit (Thermo Fisher Scientific) and exposed to FluorChem M System (ProteinSimple, CA). The protein levels were normalized with β-actin and quantified by ImageJ software (NIH, MD).

For immunofluorescence staining, cells cultured on a 24-well plate were fixed for 20 min in 4% paraformaldehyde. Then, the cells were incubated with primary antibody and Alexa Fluor 488/594-labeled secondary antibodies (Thermo Fisher Scientific). The details of the primary and secondary antibodies are provided in table S4. Nuclei were detected with DAPI (4′,6-diamidino-2-phenylindole) media and visualized using EVOS fluorescence microscopy (Thermo Fisher Scientific).

Adhesion assay

FN (Sigma-Aldrich) was coated in a final concentration of 10 μg/ml on a 48-well plate at 37°C overnight. Unbound FN was removed with PBS washing. Unspecific binding sites were blocked with 1% bovine serum albumin (BSA) for 1 hour at room temperature. Consequently, sh-ITGA5 and sh-NC hPSCs were seeded (3×10^4 cells per well) and allowed to adhere to the FN-coated plates for 30 min. Unattached cells were removed by PBS washing, and adherent cells were fixed in 4% paraformaldehyde and stained with phalloidin labeled with tetramethyl rhodamine isothiocyanate (TRITC) and DAPI. Phalloidin-labeled cells were imaged and counted.

Spheroid formation assay

Spheroids containing either sh-NC hPSCs or sh-ITGA5 hPSCs were prepared using the hanging drop method, as described elsewhere (*10*). hPSCs were suspended in culture medium to a concentration of 2.5×10^5 cells/ml. Approximately five drops (20 μl/drop, each containing 5×10^3 cells) were distributed onto a lid of a cell culture dish. Then, the lid was inverted and placed over the dish containing PBS for humidity. The spheroids were grown for 6 days and imaged under an inverted microscope. The diameter of the spheroids was measured digitally using ImageJ software.

Ninety-six–well round-bottom plates were precoated with 5% Pluronic F-127 (Sigma-Aldrich) to prevent cell attachment to the well surface. Mixed cell spheroids were generated by seeding hPSC and PANC-1/MIA PaCa-2 cells at a 1:1 ratio in a 96-well plate and incubated. The formed spheroids on third and sixth days were exposed with vehicle, AV3 (20 μM), gemcitabine (10 μM), or AV3 + gemcitabine and subsequently imaged under an inverted microscope. The diameter of the spheroids was measured digitally using ImageJ software, and then spheroid volume was calculated. On the ninth day, the heterospheroids were removed from the well plate and placed separately in single wells of a 96-well plate. CellTiter-Glo 3D reagent was added to each well, and the luminescence signal was measured after 30 min with the bioluminescent reader (Varioskan LUX, Thermo Fisher Scientific) to evaluate cell viability.

Migration assay

For the scratch assay, sh-ITGA5 and sh-NC hPSCs were seeded in a 24-well plate (6×10^4 cells per well) and allowed to become confluent.

A standardized scratch was made using a 200-μl pipette tip fixed in a custom-made holder. Then, cells were washed and incubated in fresh serum free media without growth factors. Images were captured at $t = 0$ hours and $t = 15$ hours under an inverted microscope. Images were analyzed by ImageJ software to calculate the area of the scratch and represented as the percentage of wound closure compared to control cells.

The transwell migration assay was carried out in a 24-well modified Boyden chamber kit (8-μm pores, Corning Inc., Corning, NY, USA). PANC-1 tumor cells (5×10^4) were seeded in serum-free medium in the inserts with conditioned media from sh-NC or sh-ITGA5 activated either with or without TGF-β as a chemoattractant. After 16 hours of incubation, cells that migrated on the underside of the membrane were fixed in ice-cold 100% methanol and stained with 0.1% crystal violet (Sigma-Aldrich). Migrated cells were counted in four random fields at ×100 magnification.

Cell proliferation assay

Sh-ITGA5 and sh-NC hPSCs proliferation was analyzed with a BrdU assay (Roche Life Sciences, Indianapolis, USA). Cells were plated at a density of 2.5×10^3 cells per well in a 96 well-plate. Cells were labeled using 10 μM BrdU at 37°C for 2 hours. Cells were fixed by adding FixDenat and incubated with anti–BrdU-peroxidase antibody for 90 min. The antibody was removed, cells were washed, and the substrate solution was added. The substrate product was quantified by measuring absorbance at 370 nm with a reference wavelength of 492 nm.

PANC-1 tumor cell growth was assessed by the alamarBlue assay. Conditioned media were collected from sh-NC or sh-ITGA5 PSCs with or without activation of TGF-β. PANC-1 cells were seeded at a density of 2.5×10^3 cells per well in a 96-well plate and treated with the conditioned media obtained from hPSCs. After 3 days of treatment, cells were incubated with alamarBlue (Invitrogen) at 37°C for 4 hours. Later, fluorescence reading (excitation, 540 nm; emission wavelength, 590 nm) was recorded with VICTOR (PerkinElmer, Waltham, MA).

3D collagen I gel contraction assay

A collagen suspension (5 ml) containing 3.0 ml of collagen G1 (5 mg/ml; MATRIX BioScience, Mörlenbach, Germany), 0.5 ml of 10× M199 medium (Sigma), 85 μl of 1 N NaOH (Sigma-Aldrich), and sterile water was mixed with 1.0 ml (2×10^6 cells) of sh-ITGA5 or sh-NC hPSCs. Collagen gel–cell suspension (0.6 ml per well) was plated in a 24-well culture plate and allowed to polymerize for 1 hour at 37°C. Once polymerized, 1 ml of serum-free medium was added with or without TGF-β (5 ng/ml) followed by detachment of the gels from the culture wells. To study the effect of peptidomimetic AV3, 1 ml of serum-free medium with TGF-β (5 ng/ml) and 20 μM AV3 or sAV3 peptidomimetic was added to the detached gels. Representative images were made at either 72 or 96 hours using a digital camera (Nikon, Mississauga, ON, Canada). Measurement of collagen gel diameter was performed using ImageJ imaging software (NIH, Bethesda, MD).

Cell binding assay

hPSCs or ITGA5 KD hPSCs were seeded in a 96-well plate at a density of 2.5×10^3 cells per well. The next day, cells were starved and activated either with or without TGF-β. After 24 hours, cells were washed with PBS and fixed with 4% formaldehyde (Sigma) for 15 min at room temperature. Later, fixed cells were blocked in serum-free medium with 1% BSA for 30 min at room temperature. The cells were incubated with 10 μM AV3-FAM in serum-free medium with 0.1% BSA for 60 min at room temperature. After incubation, the cells were washed with PBS, and nuclei were stained with DAPI followed by imaging using EVOS fluorescence microscope (Thermo Fisher Scientific).

Flow cytometry

hPSCs were seeded at a density of 4×10^5 cells per T25 flask. The next day, cells were starved and activated either with or without TGF-β. After 24 hours, cells were trypsinized, and cell numbers were diluted to 1×10^5 cells/ml. Cells were incubated at 37°C for 30 min to allow receptor recovery. Then, different concentrations (1, 2.5, 5, and 10 μM) of AV3-FAM were added to the suspension cells containing 2% FBS and incubated at 4°C for an hour. Cells were then centrifuged at 300*g* at 4°C for 5 min. The supernatant was decanted without disturbing the pellet, and cells were washed three times with 0.5% FBS/cold PBS and then fixed in 0.5% formaldehyde for 10 min at 4°C. Cell fluorescence was measured with flow cytometry (BD FACSCalibur).

Animal experiments and ethics statements

All the animal experiments in this study were performed according to the Institutional Animal Care and Use Committees guidelines and approved by the animal ethical committee of Utrecht University (2014.III.02.022), The Netherlands, and Central Animal Welfare (AVD1100020174305). Collection of patient tissue material was approved by the IRB of Amsterdam Medical Centre (BTC 2014_181) and performed according to the Helsinki Convention guidelines. Informed consent was obtained for all inclusions. Grafting of immunodeficient NSG mice with patient material was performed according to procedures approved by the animal experiment ethical committee (DTB102348/LEX268).

Pancreatic co-injection xenograft and PDX models

Six-week-old male CB17 SCID mice (Janvier Labs) were subcutaneously injected with PANC-1 alone (2×10^6 cells) or co-injected with hPSCs (2×10^6 cells). In another study, animals were co-injected with PANC-1 and hPSCs (2×10^6 cells) either stably transfected with sh-ITGA5 or sh-NC. The tumor growth was followed by tumor measurement using Vernier Caliper every 2 to 3 days. In a preliminary study with AV3 peptidomimetics, animals were subcutaneously co-injected with PANC-1 (2×10^6 cells) and hPSCs (4×10^6 cells). Six tumor-bearing mice per treatment group were taken and injected with either vehicle, AV3, or sAV3. Half of the group was injected intraperitoneally (20 mg/kg) and the other three intratumorally (4 mg/kg). Injections were given twice a week starting from day 9. In the next study, animals were subcutaneously co-injected either with PANC-1/MIA PaCa-2 (2×10^6 cells) or with hPSCs (4×10^6 cells). Four tumor-bearing mice per treatment group per model were taken into consideration and each group was injected with vehicle, AV3, gemcitabine, or combined treatment (AV3 + gemcitabine). After two tumor measurements, AV3 (20 mg/kg) was injected intraperitoneally thrice a week only in AV3 treatment groups. Later in all groups, injections were given twice a week. To study the effect of AV3 on the tumor perfusion, ICG (5 mg/kg) was injected via tail vein. After 24 hours of the injection, tumors were imaged using a small animal imager (Pearl Imager, LICOR, Lincoln, NE).

A freshly excised pancreatic patient tumor piece was grafted subcutaneously into the flank of immunocompromised NOD.

Cg-Prkdc^{scid}Il2rg^{tm1Wjl}/SzJ (NSG) mice with Matrigel as P1. After transplantation, tumor growth was monitored, and upon reaching a size of 800 to 1000 mm^3, PDX tumors were harvested and transplanted into the flank of NOD/SCID animals with Matrigel as P2. After that, mice with tumors reaching around 150 mm^3 were injected intraperitoneally with either vehicle, AV3 (20 mg/kg), gemcitabine (50 mg/kg), or AV3 (20 mg/kg) and gemcitabine (50 mg/kg) twice a week for 3 weeks (n = 5 mice per group).

Tumor growth was assessed with caliper every 2 to 3 days. Tumor volumes were measured using the following formula: $V = L \times B^2/2$. At the end of the experiments, animals were sacrificed under anesthesia, after which tumors were harvested and immediately snap-frozen in cold 2-methyl butane. Frozen organs were stored at −80°C until analysis. Cryosections (4 μm) were cut and fixed in acetone for 10 min before staining for collagen I and α-SMA (table S2), followed by a fluorescent secondary antibody, and the protocol was described elsewhere (*37*). The morphometric analysis was performed by a single observer in a blinded manner using standardized computer program with unbiased fixed settings. Whole-stained sections were scanned using a slide scanner (NanoZoomer) and analyzed. To specifically detect the stained area, the intensity was set in different sections and all samples were analyzed. These settings were kept constant during the analysis, and then data were divided into different groups.

Statistical analyses

Regarding survival analyses, OS was defined as the time from the date of surgery to the date of death or lost to follow-up. Kaplan-Meier estimates of the survival function, including P values from the log-rank test, were used to graphically compare the time-to-event outcomes based on ITGA5 expression and to estimate median OS. Furthermore, univariate and multivariate survival analyses were performed using the Cox proportional hazard regression model. Next to age and gender, only variables that were significant in univariate analysis were included in multivariate analyses, with an exception for primary tumor stage for OS (SPSS Statistical Software, version 23.0; IBM SPSS Inc., Chicago, IL). Group data are presented as means ± SEM for at least three independent experiments. The graphs and statistical analyses were performed using GraphPad Prism version 5.02 (GraphPad Prism Software Inc., La Jolla, CA). Statistical analysis of the results was performed by either a two-tailed unpaired Student's t test for comparison of two treatment groups or a one-way analysis of variance (ANOVA) to compare multiple treatment groups. In all cases, differences were considered significant at $P < 0.05$.

SUPPLEMENTARY MATERIALS

Supplementary material for this article is available at http://advances.sciencemag.org/cgi/content/full/5/9/eaax2770/DC1

Fig. S1. Effect of ITGA5 knockdown in hPSCs on α-SMA, collagen I expression, and downstream genes.
Fig. S2. Effect of ITGA5 blocking peptidomimetic (AV3) (related to Fig. 4).
Fig. S3. AV3 reduces PSC-induced pancreatic tumor growth in the subcutaneous co-injection (PANC-1 + hPSCs) pancreatic tumor model.
Fig. S4. Effect of AV3 in PANC-1 and MIA PaCa-2 tumor models.
Fig. S5. Characterization of human pancreatic tumor tissue for PDX and PDX models.
Table S1. Characteristics for PDAC patients.
Table S2. Univariable and multivariable Cox proportional hazard model predictive value of ITGA5 expression on OS of patients with PDAC.
Table S3. Primers used for quantitative real-time PCR.
Table S4. Details of the antibodies used for Western blot analyses.
Data file S1. The complete gene array data on sh-ITGA5 hPSCs versus sh-NC and the effect of TGF-β activation on sh-NC and sh-ITGA5 hPSCs.

REFERENCES AND NOTES

1. R. L. Siegel, K. D. Miller, A. Jemal, Cancer statistics, 2017. *CA Cancer J. Clin.* **67**, 7–30 (2017).
2. A. Neesse, P. Michl, K. K. Frese, C. Feig, N. Cook, M. A. Jacobetz, M. P. Lolkema, M. Buchholz, K. P. Olive, T. M. Gress, D. A. Tuveson, Stromal biology and therapy in pancreatic cancer. *Gut* **60**, 861–868 (2011).
3. M. F. Bijlsma, H. W. M. van Laarhoven, The conflicting roles of tumor stroma in pancreatic cancer and their contribution to the failure of clinical trials: A systematic review and critical appraisal. *Cancer Metastasis Rev.* **34**, 97–114 (2015).
4. C. Feig, A. Gopinathan, A. Neesse, D. S. Chan, N. Cook, D. A. Tuveson, The pancreas cancer microenvironment. *Clin. Cancer Res.* **18**, 4266–4276 (2012).
5. A. Vonlaufen, S. Joshi, C. Qu, P. A. Phillips, Z. Xu, N. R. Parker, C. S. Toi, R. C. Pirola, J. S. Wilson, D. Goldstein, M. V. Apte, Pancreatic stellate cells: Partners in crime with pancreatic cancer cells. *Cancer Res.* **68**, 2085–2093 (2008).
6. M. G. Bachem, E. Schneider, H. Groß, H. Weidenbach, R. M. Schmid, A. Menke, M. Siech, H. Beger, A. Grünert, G. Adler, Identification, culture, and characterization of pancreatic stellate cells in rats and humans. *Gastroenterology* **115**, 421–432 (1998).
7. J. Schnittert, R. Bansal, J. Prakash, Targeting pancreatic stellate cells in cancer. *Trends Cancer* **5**, 128–142 (2019).
8. M. V. Apte, S. Park, P. A. Phillips, N. Santucci, D. Goldstein, R. K. Kumar, G. A. Ramm, M. Buchler, H. Friess, J. A. McCarroll, G. Keogh, N. Merrett, R. Pirola, J. S. Wilson, Desmoplastic reaction in pancreatic cancer: Role of pancreatic stellate cells. *Pancreas* **29**, 179–187 (2004).
9. M. V. Apte, J. S. Wilson, A. Lugea, S. J. Pandol, A starring role for stellate cells in the pancreatic cancer microenvironment. *Gastroenterology* **144**, 1210–1219 (2013).
10. P. R. Kuninty, L. Bojmar, V. Tjomsland, M. Larsson, G. Storm, A. Östman, P. Sandström, J. Prakash, MicroRNA-199a and -214 as potential therapeutic targets in pancreatic stellate cells in pancreatic tumor. *Oncotarget* **7**, 16396–16408 (2016).
11. J. Schnittert, M. A. Heinrich, P. R. Kuninty, G. Storm, J. Prakash, Reprogramming tumor stroma using an endogenous lipid lipoxin A4 to treat pancreatic cancer. *Cancer Lett.* **420**, 247–258 (2018).
12. D. F. Mardhian, G. Storm, R. Bansal, J. Prakash, Nano-targeted relaxin impairs fibrosis and tumor growth in pancreatic cancer and improves the efficacy of gemcitabine in vivo. *J. Control. Release* **290**, 1–10 (2018).
13. B. C. Özdemir, T. Pentcheva-Hoang, J. L. Carstens, X. Zheng, C.-C. Wu, T. R. Simpson, H. Laklai, H. Sugimoto, C. Kahlert, S. V. Novitskiy, A. De Jesus-Acosta, P. Sharma, P. Heidari, U. Mahmood, L. Chin, H. L. Moses, V. M. Weaver, A. Maitra, J. P. Allison, V. S. LeBleu, R. Kalluri, Depletion of carcinoma-associated fibroblasts and fibrosis induces immunosuppression and accelerates pancreas cancer with reduced survival. *Cancer Cell* **25**, 719–734 (2014).
14. A. D. Rhim, P. E. Oberstein, D. H. Thomas, E. T. Mirek, C. F. Palermo, S. A. Sastra, E. N. Dekleva, T. Saunders, C. P. Becerra, I. W. Tattersall, C. B. Westphalen, J. Kitajewski, M. G. Fernandez-Barrena, M. E. Fernandez-Zapico, C. Iacobuzio-Donahue, K. P. Olive, B. Z. Stanger, Stromal elements act to restrain, rather than support, pancreatic ductal adenocarcinoma. *Cancer Cell* **25**, 735–747 (2014).
15. R. O. Hynes, Integrins: Bidirectional, allosteric signaling machines. *Cell* **110**, 673–687 (2002).
16. J. Schnittert, R. Bansal, G. Storm, J. Prakash, Integrins in wound healing, fibrosis and tumor stroma: High potential targets for therapeutics and drug delivery. *Adv. Drug Deliv. Rev.* **129**, 37–53 (2018).
17. J. Schnittert, R. Bansal, D. F. Mardhian, J. van Baarlen, A. Östman, J. Prakash, Integrin α11 in pancreatic stellate cells regulates tumor stroma interaction in pancreatic cancer. *FASEB J.* **33**, 6609–6621 (2019).
18. F. Schaffner, A. M. Ray, M. Dontenwill, Integrin α5β1, the fibronectin receptor, as a pertinent therapeutic target in solid tumors. *Cancers* **5**, 27–47 (2013).
19. J. S. Desgrosellier, D. A. Cheresh, Integrins in cancer: Biological implications and therapeutic opportunities. *Nat. Rev. Cancer* **10**, 9–22 (2010).
20. G. Biffi, T. E. Oni, B. Spielman, Y. Hao, E. Elyada, Y. Park, J. Preall, D. A. Tuveson, IL1-induced JAK/STAT signaling is antagonized by TGFβ to shape CAF heterogeneity in pancreatic ductal adenocarcinoma. *Cancer Discov.* **9**, 282–301 (2019).
21. J. Franco-Barraza, R. Francescone, T. Luong, N. Shah, R. Madhani, G. Cukierman, E. Dulaimi, K. Devarajan, B. L. Egleston, E. Nicolas, R. Katherine Alpaugh, R. Malik, R. G. Uzzo, J. P. Hoffman, E. A. Golemis, E. Cukierman, Matrix-regulated integrin $\alpha_v\beta_5$ maintains $\alpha_5\beta_1$-dependent desmoplastic traits prognostic of neoplastic recurrence. *eLife* **6**, e20600 (2017).
22. C. Margadant, A. Sonnenberg, Integrin–TGF-β crosstalk in fibrosis, cancer and wound healing. *EMBO Rep.* **11**, 97–105 (2010).
23. H. Tian, K. Mythreye, C. Golzio, N. Katsanis, G. C. Blobe, Endoglin mediates fibronectin/$\alpha_5\beta_1$ integrin and TGF-β pathway crosstalk in endothelial cells. *EMBO J.* **31**, 3885–3900 (2012).
24. M. G. Bachem, M. Schünemann, M. Ramadani, M. Siech, H. Beger, A. Buck, S. Zhou, A. Schmid-Kotsas, G. Adler, Pancreatic carcinoma cells induce fibrosis by stimulating proliferation and matrix synthesis of stellate cells. *Gastroenterology* **128**, 907–921 (2005).

25. C. Strell, K. J. Norberg, A. Mezheyeuski, J. Schnittert, P. R. Kuninty, C. F. Moro, J. Paulsson, N. A. Schultz, D. Calatayud, J. M. Löhr, O. Frings, C. S. Verbeke, R. L. Heuchel, J. Prakash, J. S. Johansen, A. Östman, Stroma-regulated HMGA2 is an independent prognostic marker in PDAC and AAC. *Br. J. Cancer* **117**, 65–77 (2017).
26. M. Nagae, S. Re, E. Mihara, T. Nogi, Y. Sugita, J. Takagi, Crystal structure of $\alpha5\beta1$ integrin ectodomain: Atomic details of the fibronectin receptor. *J. Cell Biol.* **197**, 131–140 (2012).
27. M. Yamauchi, T. H. Barker, D. L. Gibbons, J. M. Kurie, The fibrotic tumor stroma. *J. Clin. Invest.* **128**, 16–25 (2018).
28. J. Gong, D. Wang, L. Sun, E. Zborowska, J. K. V. Willson, M. G. Brattain, Role of $\alpha_5\beta_1$ integrin in determining malignant properties of colon carcinoma cells. *Cell Growth Differ.* **8**, 83–90 (1997).
29. J.-M. Nam, Y. Onodera, M. J. Bissell, C. C. Park, Breast cancer cells in three-dimensional culture display an enhanced radioresponse after coordinate targeting of integrin $\alpha5\beta1$ and fibronectin. *Cancer Res.* **70**, 5238–5248 (2010).
30. M. Sinn, C. Denkert, J. K. Striefler, U. Pelzer, J. M. Stieler, M. Bahra, P. Lohneis, B. Dörken, H. Oettle, H. Riess, B. V. Sinn, α-Smooth muscle actin expression and desmoplastic stromal reaction in pancreatic cancer: Results from the CONKO-001 study. *Br. J. Cancer* **111**, 1917–1923 (2014).
31. S. Yuzawa, M. R. Kano, T. Einama, H. Nishihara, PDGFRβ expression in tumor stroma of pancreatic adenocarcinoma as a reliable prognostic marker. *Med. Oncol.* **29**, 2824–2830 (2012).
32. B. Costa-Silva, N. M. Aiello, A. J. Ocean, S. Singh, H. Zhang, B. K. Thakur, A. Becker, A. Hoshino, M. T. Mark, H. Molina, J. Xiang, T. Zhang, T.-M. Theilen, G. García-Santos, C. Williams, Y. Ararso, Y. Huang, G. Rodrigues, T.-L. Shen, K. J. Labori, I. M. B. Lothe, E. H. Kure, J. Hernandez, A. Doussot, S. H. Ebbesen, P. M. Grandgenett, M. A. Hollingsworth, M. Jain, K. Mallya, S. K. Batra, W. R. Jarnagin, R. E. Schwartz, I. Matei, H. Peinado, B. Z. Stanger, J. Bromberg, D. Lyden, Pancreatic cancer exosomes initiate pre-metastatic niche formation in the liver. *Nat. Cell Biol.* **17**, 816–826 (2015).
33. I. Ozaki, H. Hamajima, S. Matsuhashi, T. Mizuta, Regulation of TGF-$\beta1$-induced pro-apoptotic signaling by growth factor receptors and extracellular matrix receptor integrins in the liver. *Front. Physiol.* **2**, 78 (2011).
34. T. Cai, Q.-Y. Lei, L.-Y. Wang, X.-L. Zha, TGF-$\beta1$ modulated the expression of $\alpha5\beta1$ integrin and integrin-mediated signaling in human hepatocarcinoma cells. *Biochem. Biophys. Res. Commun.* **274**, 519–525 (2000).
35. N. Yoshida, A. Masamune, S. Hamada, K. Kikuta, T. Takikawa, F. Motoi, M. Unno, T. Shimosegawa, Kindlin-2 in pancreatic stellate cells promotes the progression of pancreatic cancer. *Cancer Lett.* **390**, 103–114 (2017).
36. E. C. Connolly, J. Freimuth, R. J. Akhurst, Complexities of TGF-β targeted cancer therapy. *Int. J. Biol. Sci.* **8**, 964–978 (2012).
37. R. Bansal, T. Tomar, A. Östman, K. Poelstra, J. Prakash, Selective targeting of Interferon γ to stromal fibroblasts and pericytes as a novel therapeutic approach to inhibit angiogenesis and tumor growth. *Mol. Cancer Ther.* **11**, 2419–2428 (2012).

Acknowledgments: We thank C. Waasdorp (Academic Medical Centre, The Netherlands) and B. Klomphaar (University of Twente) for their technical assistance in animal experiments. **Funding:** This study was supported by the Swedish Research Council, Stockholm (project no. 2011-5389), and The Netherlands Organisation for Scientific Research (NWO-STW) Phase-2 grant 2017/STW/00364810 to J.P. and KWF Dutch Cancer Society grants UVA 2012-5607 and UVA 2013-5932 to M.F.B. and H.W.v.L. **Author contribution:** P.R.K. designed, performed, analyzed, and interpreted the experimental data and wrote the manuscript. J.v.B. provided the tumor slides for histochemical staining. R.B. assisted in in vivo experiments and data analysis and critically reviewed the manuscript. D.F.M. and J.S. contributed in the in vivo experiments. G.S., J.M.M., and A.Ö. read and gave inputs to the manuscript. M.F.B. and H.W.v.L. provided the PDX pancreatic tumor sample and gave input to the manuscript. S.W.L.D.G., P.J.K.K., A.L.V., and C.F.M.S. contributed to the clinical patient data and interpreted and analyzed the data. J.P. led the whole study including design of the study, interpretation of the results, and writing and editing of the manuscript. **Competing interests:** J.P. is the founder of and a shareholder of ScarTec Therapeutics BV. J.M.M. is a shareholder in ScarTec Therapeutics. M.F.B. has received research funding from Celgene; this party was not involved in the drafting of the manuscript. H.W.v.L. has received research grants from Bayer Schering Pharma AG, Bristol-Myers Squibb, Celgene, Eli Lilly and Company, Nordic Pharma Group, Philips, and Roche Pharmaceuticals; none of these parties was not involved in the drafting of the manuscript. M.F.B. has acted as a consultant to Servier; this party was not involved in drafting of the manuscript. H.W.v.L. has acted as a consultant for Bristol-Myers Squibb, Eli Lilly and Company, and Nordic Pharma Group; none of these parties was not involved in drafting of the manuscript. J.P. is an inventor of a patent related to this work filed by the University of Twente (no. PCT/NL2016/050725, filed on 21 October 2016). The other authors declare that they have no competing interests. **Data and materials availability:** All data needed to evaluate the conclusions in the paper are present in the paper and/or the Supplementary Materials. Additional data related to this paper may be requested from the authors. The PDX tissue can be provided by a pending scientific review of M.F.B. and H.W.v.L. (Amsterdam University Medical Centre) and a completed material transfer agreement. Requests for the PDX tissue should be submitted to M.F.B. and H.W.v.L.

Submitted 8 March 2019
Accepted 5 August 2019
Published 4 September 2019
10.1126/sciadv.aax2770

Citation: P. R. Kuninty, R. Bansal, S. W. L. De Geus, D. F. Mardhian, J. Schnittert, J. van Baarlen, G. Storm, M. F. Bijlsma, H. W. van Laarhoven, J. M. Metselaar, P. J. K. Kuppen, A. L. Vahrmeijer, A. Östman, C. F. M. Sier, J. Prakash, ITGA5 inhibition in pancreatic stellate cells attenuates desmoplasia and potentiates efficacy of chemotherapy in pancreatic cancer. *Sci. Adv.* **5**, eaax2770 (2019).

ITGA5 inhibition in pancreatic stellate cells attenuates desmoplasia and potentiates efficacy of chemotherapy in pancreatic cancer

Praneeth R. Kuninty, Ruchi Bansal, Susanna W. L. De Geus, Deby F. Mardhian, Jonas Schnittert, Joop van Baarlen, Gert Storm, Maarten F. Bijlsma, Hanneke W. van Laarhoven, Josbert M. Metselaar, Peter J. K. Kuppen, Alexander L. Vahrmeijer, Arne Östman, Cornelis F. M. Sier and Jai Prakash

Sci Adv **5** (9), eaax2770.
DOI: 10.1126/sciadv.aax2770